Cell Reports
Physical Science

Article

# Co-harvesting universe coldness and solar energy for tri-generation of cooling, electricity, and heating

## Graphical abstract

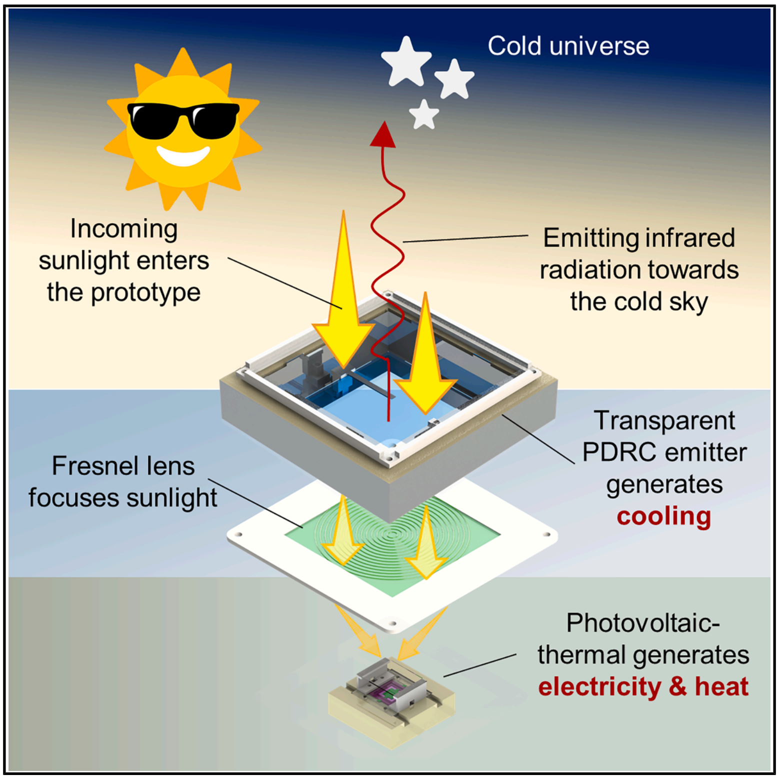


## Highlights

- Hybrid technologies co-harvest universe coldness and solar energy
- The prototype delivers electricity, 6.5°C sub-ambient cooling, and 110°C heat
- The tandem design produces 266°C heat while maintaining sub-ambient cooling


## Authors

Iván Alberto Cruz García, Botho Lehmann, Shanhui Fan, Gan Huang

## Correspondence

shanhui@stanford.edu (S.F.),
gan.huang@kit.edu (G.H.)



## In brief

Cruz et al. introduce a hybrid solar passive radiative cooling prototype that co-harvests universe coldness and solar energy. By thermally decoupling the transparent radiative cooler from the solar heat generation unit, the system delivers cooling, electricity, and heat from the same area at the same time.


Cruz García et al., 2026, Cell Reports Physical Science 7, 103492
August 19, 2026 
https://doi.org/10.1016/j.xcrp.2026.103492

Cell Reports
Physical Science

CellPress
OPEN ACCESS

Article

# Co-harvesting universe coldness and solar energy for tri-generation of cooling, electricity, and heating

Iván Alberto Cruz García,[1] Botho Lehmann,[1] Shanhui Fan,[2,*] and Gan Huang[1,3,*]
[1]Institute of Microstructure Technology, Karlsruhe Institute of Technology, Hermann-von-Helmholtz-Platz 1, 76344 Eggenstein-Leopoldshafen, Germany
[2]Department of Electrical Engineering, Stanford University, Stanford, CA, USA
[3]Lead contact
*Correspondence: shanhui@stanford.edu (S.F.), gan.huang@kit.edu (G.H.)
https://doi.org/10.1016/j.xcrp.2026.103492

## SUMMARY

Passive daytime radiative cooling (PDRC) provides sustainable sub-ambient cooling, yet most PDRC designs reject incident sunlight that could otherwise be harvested. Here, we introduce hybrid PDRC-solar technologies that co-harvest universe coldness and solar energy to deliver cooling, electricity, and heating from the same area at the same time. The system combines a transparent PDRC emitter, which permits solar transmission, with a tandem concentrated photovoltaic-thermal collector on a two-axis solar tracker. The transparent PDRC emitter achieves cooling of 6.5°C below ambient, while the photovoltaic-thermal collector produces 60.6 W/m$^2$ of electricity and stores heat reaching 110.8°C. Replacing the photovoltaic-thermal collector with a spectrally selective solar-thermal absorber increases the stored temperature to 266.8°C, while the emitter maintains cooling of 2.4°C below ambient. This simultaneous harvesting is enabled by decoupling light intensity and limiting thermal exchange between the colder PDRC emitter and the hotter solar collector.

## INTRODUCTION

More than 75% of global greenhouse gas emissions originate from the energy sector.[1] Buildings are among the largest energy consumers, accounting for 30% of global final energy use and 26% of energy-related emissions.[2] In Europe and North America, the share rises to about 40%.[3] Heating, cooling, and electricity for lighting and appliances dominate building energy demand. Clean provision of these services is essential for achieving the net zero emissions by 2050 scenario.[2]

Solar energy technologies provide clean electricity and heating and have seen rapid progress in recent decades. Photovoltaics supply renewable electricity.[4,5] Global photovoltaic capacity reached 2,000 gigawatts in 2025[4] and is expected to drive most renewable expansion in the coming years.[6] Solar-thermal collectors convert sunlight directly into heat, and hybrid photovoltaic-thermal solar collectors recover the waste heat produced in photovoltaic modules to deliver both electricity and thermal energy.[7] Together, these technologies form the backbone of solar-based building energy systems.

Meeting cooling demand sustainably presents additional challenges. Passive daytime radiative cooling (PDRC) has emerged as a promising approach by using the cold universe as the heat sink.[8–10] PDRC materials exploit the atmospheric window between 8 and 13 μm where the atmosphere is more transparent to infrared radiation.[8,11] They are typically engineered to exhibit high emissivity within this window to radiate heat to outer space and high reflectivity across the solar spectrum to suppress solar heating, enabling sub-ambient cooling without energy input.[12–14] Over the past decade, a wide range of PDRC materials has been developed,[14,15] with milestones including multilayer nanophotonic emitters,[10] single-layer polymers on reflectors,[16,17] porous polymers,[18–20] textile,[21–23] and porous ceramics.[24,25] Recent work has also extended PDRC to vertical surfaces.[26,27]

Both solar harvesting and PDRC require access to building surfaces, especially roofs, which are limited.[28] Rather than competing for area, it is desirable to co-harvest universe coldness and solar energy simultaneously (i.e., from the same area and at the same time). Theoretical analysis has shown the great thermodynamic potential of co-harvesting these two energy sources.[29] A pioneering experimental study demonstrated simultaneous PDRC (29°C below the ambient) and solar heating (24°C above the ambient) by placing a mid-infrared (MIR) transparent absorber above a PDRC emitter within a vacuum condition.[30] By positioning the PDRC emitter vertically between V-shaped spectrally selective solar-thermal absorbers, the system produces heat at about 30°C above ambient.[31] A reversed configuration places a sunlight-transparent PDRC emitter above a solar harvester separated by a gap, but previous simulations indicate that significant thermal exchange between the cold PDRC emitter and hot solar collector restricts the ability to achieve both sub-ambient cooling and valuable high-temperature heat.[32] In this arrangement, the solar collector temperature is limited to only 33.9°C if sub-ambient cooling is to be maintained.[32] These previous studies highlight the difficulty of simultaneously achieving sub-ambient cooling and high-temperature heat generation. Instead of producing heat, a more recent experiment integrated a photovoltaic cell beneath a transparent PDRC emitter and achieved co-generation of cooling and electricity,[33] and another study used transparent PDRC emitter for cooling and indoor lightening.[34]

However, despite these advances, approaches for simultaneously producing sub-ambient cooling together with valuable high-temperature heat remain lacking. Moreover, full tri-generation of sub-ambient cooling, electricity, and high-grade heat from the same area and at the same time has not yet been demonstrated. Achieving these combined functionalities would create opportunities for integrated building energy systems and compact multifunctional solar devices, where limited surface areas can be used to provide multiple energy services.

In this study, we develop a hybrid PDRC-solar system (PDRCS) that co-harvests universe coldness and solar energy. Compared with previous radiative cooling-solar hybrid studies that mainly focused on dual generation, the proposed PDRCS is designed to achieve tri-generation of sub-ambient cooling, electricity, and high-temperature heat above 100°C from the same area and at the same time. This capability is enabled by the integration of a transparent PDRC emitter, solar concentration, and thermal decoupling between the cold emitter and the hot solar collector. A transparent PDRC emitter provides sub-ambient cooling while allowing sunlight to pass through and be concentrated by a Fresnel lens onto a gallium arsenide (GaAs)-based concentrated photovoltaic-thermal collector mounted on a two-axis solar tracker. The system achieves 6.5°C sub-ambient cooling, 60.6 W/m$^2$ of electricity, and heating up to 110.8°C. Replacing the photovoltaic-thermal collector with a spectrally selective solar-thermal absorber enables temperatures up to 266.8°C while maintaining 2.4°C sub-ambient cooling. These results demonstrate the potential of co-utilizing universe coldness and solar heat to deliver combined cooling, electricity, and high-temperature heating from the same area at the same time.

## RESULTS

### The concept and design of the hybrid PDRCS collector for tri-generation

The PDRCS consists of a tandem configuration in which a transparent PDRC emitter is placed above a concentrated solar photovoltaic-thermal collector for tri-generation of cooling, electricity, and heating, as illustrated in Figure 1A. This tri-generation strategy enables simultaneous use of universe coldness and the full solar spectrum. The transparent PDRC emitter harvests coldness from the universe to provide cooling. The photovoltaic cells convert short-wavelength solar photons into electricity, while the longer-wavelength solar photons that are not useful for electrical generation are used for heat production instead of contributing to photovoltaic overheating.

The PDRC emitter on the top layer provides cooling by emitting MIR radiation to the cold universe. To enhance the cooling performance, MIR reflectors are positioned around the emitter to block radiation from the ground when the system tilts during solar tracking and to reduce downwelling atmospheric radiation. The MIR reflectors have low emissivity on both sides in the MIR range, which minimizes radiation heat exchange between the MIR reflectors and the PDRC emitter.

Sunlight transmitted through the transparent PDRC emitter is concentrated onto a photovoltaic-thermal collector to generate electricity and heat. Such concentration configuration significantly reduces the view factor for radiative exchange between the cold PDRC emitter and the hot solar collector, thereby lowering the thermal interaction. The intensified solar flux also permits higher-temperature heat output. An intermediate radiation barrier that is transparent to sunlight but opaque to MIR is inserted to further limit radiative exchange.

As summarized in Figure 1B, standalone photovoltaics harvest only the portion below the bandgap wavelength (e.g., <0.87 μm for GaAs), while the remaining long-wavelength photons contribute to waste heat. Standalone PDRC relies on the 8 to 13 μm atmospheric window. The hybrid PDRCS in this study is designed to utilize both the full solar spectrum and MIR atmospheric window range, enabling simultaneous harvesting of universe coldness and solar energy.

The exploded view is shown in Figure 1C. One 210 × 297-mm MIR reflector is vertically installed on the south side. Two 148 × 210-mm MIR reflectors are mounted on the east and west sides at an angle of 40°. The north side is left open. This configuration blocks ground radiation during solar tracking. The 10 × 10-cm transparent PDRC emitter is composed of a 1-mm-thick silica substrate uniformly coated with a 70-μm-thick polydimethylsiloxane (PDMS) layer. A 10 × 10-cm Fresnel lens with a focal length of 50 mm concentrates sunlight onto a 1 × 1-cm GaAs-based photovoltaic-thermal collector. The full PDRCS assembly is mounted on a two-axis solar tracking platform (Figure S1).

### Performance of the transparent PDRC emitter chamber

The transparent PDRC emitter chamber forms the first stage of the PDRCS, so its performance under different operating conditions should be evaluated. As shown in Figure 2A, the PDRC emitter is positioned at the center of the chamber, and the internal walls are lined with aluminum films to suppress solar heating. A sun-shielded thermocouple is attached to the top surface of the emitter (Figure S2). The chamber is insulated by a 2-cm-thick thermal-insulation foam. A low-density polyethylene (LDPE) film is mounted on the top as a wind shield.

The PDRC emitter has an optical transmittance of 94% in the solar spectrum (Figure 2B), allowing incident sunlight to reach the downstream solar collector. It also exhibits negligible absorption in the 0.3- to 2.5-μm and a high emissivity of 0.95 in the 8- to 13-μm atmospheric window, confirming its suitability as a transparent PDRC emitter. The optical properties of other components in the chamber, including the LDPE film, polymethyl-methacrylate Fresnel lens, aluminum reflector, and silica wafer, are provided in Figure S3. About 63% of incident sunlight passes through the PDRC emitter chamber for the downstream solar collector, as shown in Figure 2C.

CellPress
OPEN ACCESS

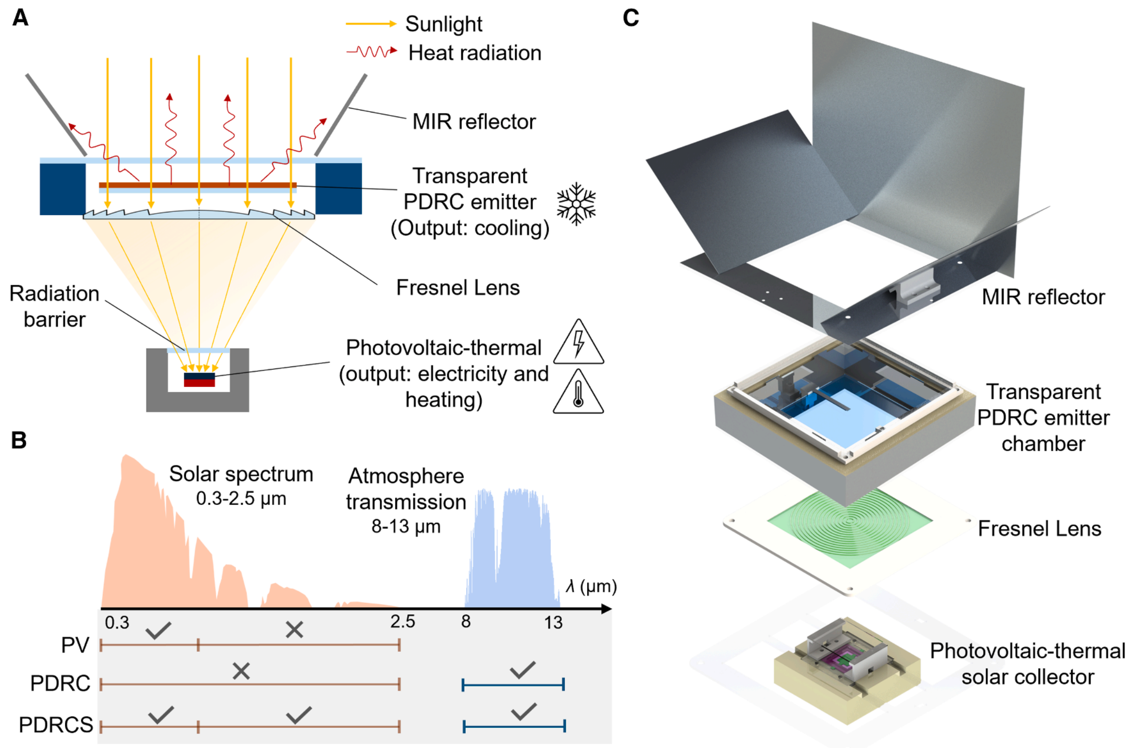


**Figure 1. Concept and design of the hybrid PDRCS collector for tri-generation**

(A) Schematic of the PDRCS collector. A transparent PDRC emitter radiates heat to the cold universe to provide sub-ambient cooling. Sunlight transmitted through the emitter is concentrated by a Fresnel lens onto a solar photovoltaic-thermal module that generates electricity and heat. A mid-infrared (MIR) reflector enhances cooling by blocking radiation from the ground, and a radiation barrier reduces thermal exchange between the PDRC emitter and the photovoltaic-thermal module. This tri-generation strategy enables simultaneous and optimal use of universe coldness and also the full solar spectrum.

(B) Comparison of spectral utilization. Standalone photovoltaics harvest only the solar spectrum (0.3–2.5 μm), and standalone PDRC harvests only the atmospheric window (8–13 μm). The PDRCS is designed to utilize both ranges simultaneously. The transparent PDRC emitter harvests coldness from the universe to provide cooling. The photovoltaic cells convert short-wavelength solar photons into electricity, while the longer-wavelength solar photons that are not useful for electrical generation are used for heat production instead of contributing to photovoltaic overheating.

(C) Exploded three dimensional view of the PDRCS structure.

The PDRC emitter chamber was tested at the Solar Park of the Karlsruhe Institute of Technology (Eggenstein-Leopoldshafen, Germany) on 11 April 2025. The sunlight transmitted through the chamber was reflected away using an inclined aluminum reflector. Three operating configurations were examined sequentially, as shown in Figure 2D. Corresponding weather conditions, including solar irradiance and humidity, are presented in Figure 2E. The solar irradiance shown in Figure 2E corresponds to the in-plane irradiance measured on the PDRCS surface during two-axis solar tracking. Because the prototype was continuously adjusted to face the sun, the measured irradiance remained high. For comparison, the horizontal solar irradiance without solar tracking is provided in Figure S5.

In phase I (09:50 to 10:37), the PDRC emitter remained horizontal and directly faced the sky, with the MIR reflectors installed. Before 09:50, the transparent PDRC emitter was covered by an opaque lid, which blocked exposure to the cold sky and suppressed radiative cooling. This procedure was used to establish a controlled initial condition in which the PDRC emitter temperature was close to ambient temperature before the experiment started. After the lid was removed at 09:50, the emitter was exposed to the cold sky and began radiative cooling, causing the rapid temperature decrease observed at the beginning of phase I. The temperature continued to decrease for approximately 15 min before reaching a more stable condition. The emitter achieved a maximum cooling of 13.6°C below ambient at 10:21 despite the humidity being as high as 72%. This confirms that PDMS-coated silica functions as an effective transparent PDRC emitter. We further conducted a repeated experiment with a longer steady-state testing duration from 09:15 to 11:15. The repeated test showed a similar temperature evolution and maintained stable sub-ambient cooling of approximately 13°C for more than 1.5 h (Figure S4).

In phase II (10:37 to 15:47), the two-axis solar tracker was activated, so the PDRC emitter continuously faced the sun. Solar irradiance rose sharply and then stabilized above 1,000 W/m$^2$. The increased solar load raised the temperature of the emitter, and at 13:00 the emitter was 2.5°C below ambient. As humidity decreased to about 40%, the cooling performance improved, and, at 15:00, the emitter reached 9.4°C below ambient. Lower humidity reduces atmospheric thermal radiation, which

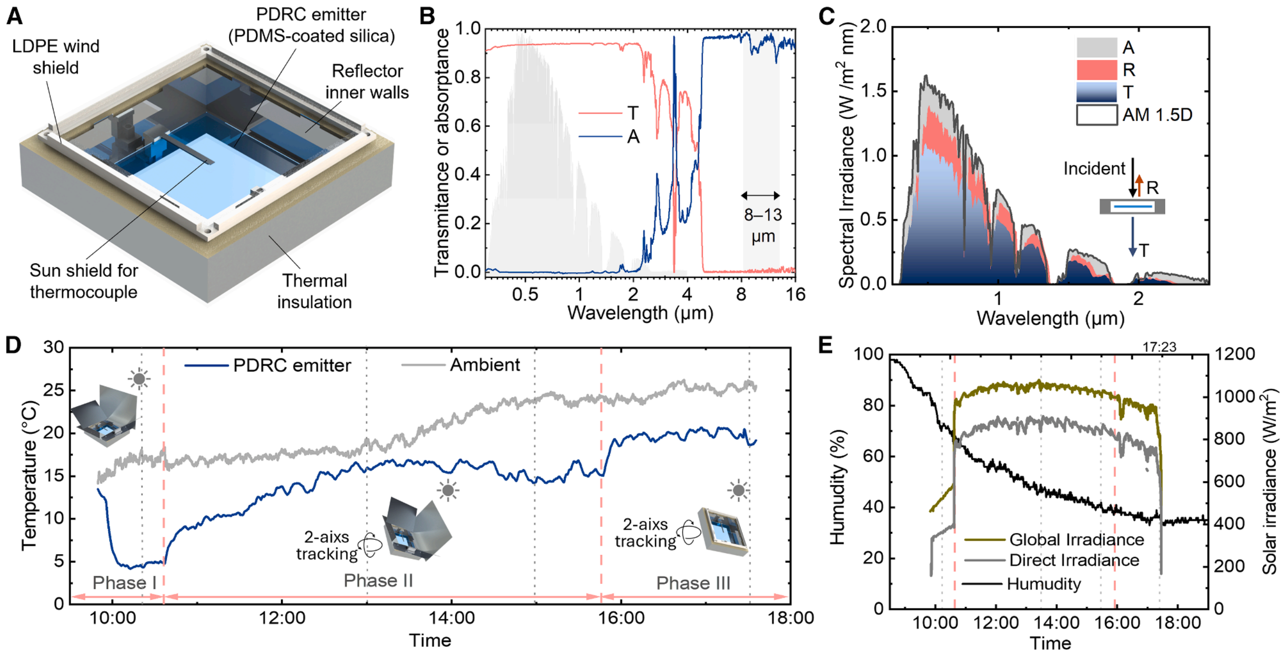


**Figure 2. Optical properties and cooling performance of the transparent PDRC emitter**

(A) Structure of the transparent PDRC emitter chamber. The emitter is positioned at the center of the chamber, whose inner walls are lined with polished aluminum reflectors and outer walls are insulated. A thermocouple attached to the emitter surface is shaded by an aluminum sunshield to reduce measurement error.

(B) Transmittance (*T*) and absorptance (*A*) of the transparent PDRC emitter (PDMS-coated silica). The emitter exhibits high solar transmittance and high emissivity in the atmospheric window.

(C) Fractions of incident sunlight (AM1.5D spectrum) transmitted (*T*), reflected (*R*), and absorbed (*A*) by the complete PDRC emitter chamber.

(D) Cooling performance of the standalone PDRC emitter under three configurations. Phase I: emitter fixed horizontally toward the sky with MIR reflectors. Phase II: emitter tracking the sun with MIR reflectors. Phase III: emitter tracking the sun without MIR reflectors.

(E) Measured global and diffuse solar irradiance and ambient humidity during the experiment. Vertical dashed red lines indicate the transitions between phase I, phase II, and phase III, while vertical dotted gray lines mark the specific time points discussed in the main text.

strengthens net radiative cooling. At 15:00, the solar elevation angle was 44°, corresponding to an emitter tilt of 46°, where the MIR reflectors effectively suppressed radiation from the ground.

Phase III began at 15:47, and the MIR reflectors were removed while solar tracking continued. The temperature of the PDRC emitter increased immediately by approximately 4°C within 10 min because of enhanced absorption of thermal radiation from the ground and surrounding surfaces after removing the MIR reflector. During this short transition period, the weather conditions remained nearly unchanged, indicating that the PDRC emitter temperature increase was primarily caused by removal of the MIR reflectors rather than environmental fluctuations. Removal of the MIR reflectors led to weaker sub-ambient cooling than that observed in phase II. At 17:30, the emitter was 7.4°C below ambient, which is worse than in phase II. This highlights the essential role of the MIR reflectors in reducing environmental radiation gain. To further verify this effect, we conducted an additional comparison experiment in which two PDRC emitter setups, with and without MIR reflectors, were tested simultaneously under the same environmental conditions and time window. The PDRC emitter equipped with MIR reflectors consistently exhibited significantly stronger cooling performance (Figure S4). This confirms that the MIR reflectors effectively suppress environmental radiation gain.

## Tri-generation performance of the hybrid PDRCS prototype

The photovoltaic-thermal module was then integrated beneath the transparent PDRC emitter, and the full prototype was mounted on the same two-axis solar tracker, as shown in Figure 3A. The configuration of the photovoltaic-thermal module is detailed in Figure 3B. A GaAs solar cell was selected because it is well suited for high-concentration and high-temperature operation. A copper block with dimensions of 1 × 1 × 1 cm was attached to the underside of the GaAs cell to function as the thermal storage element. A 0.5-mm-thick silica film was used as the radiation barrier and positioned above the GaAs cell to limit radiative coupling with the transparent PDRC emitter. A photograph of the complete PDRCS prototype is shown in Figure 3C.

The outdoor testing was conducted on 7 April 2025. The cooling performance of the transparent PDRC emitter is shown in Figure 3D, and the heating and electrical performance of the photovoltaic-thermal module at the same time is presented in Figure 3E. The PDRC emitter reached 6.5°C below ambient at 16:04, while the downstream photovoltaic-thermal collector reached 110.8°C and produced 60.6 W/m$^2$ of electricity. The electrical efficiency is calculated per unit area of the overall incident sunlight (i.e., PDRC emitter area). These results demonstrate successful tri-generation of sub-ambient cooling,

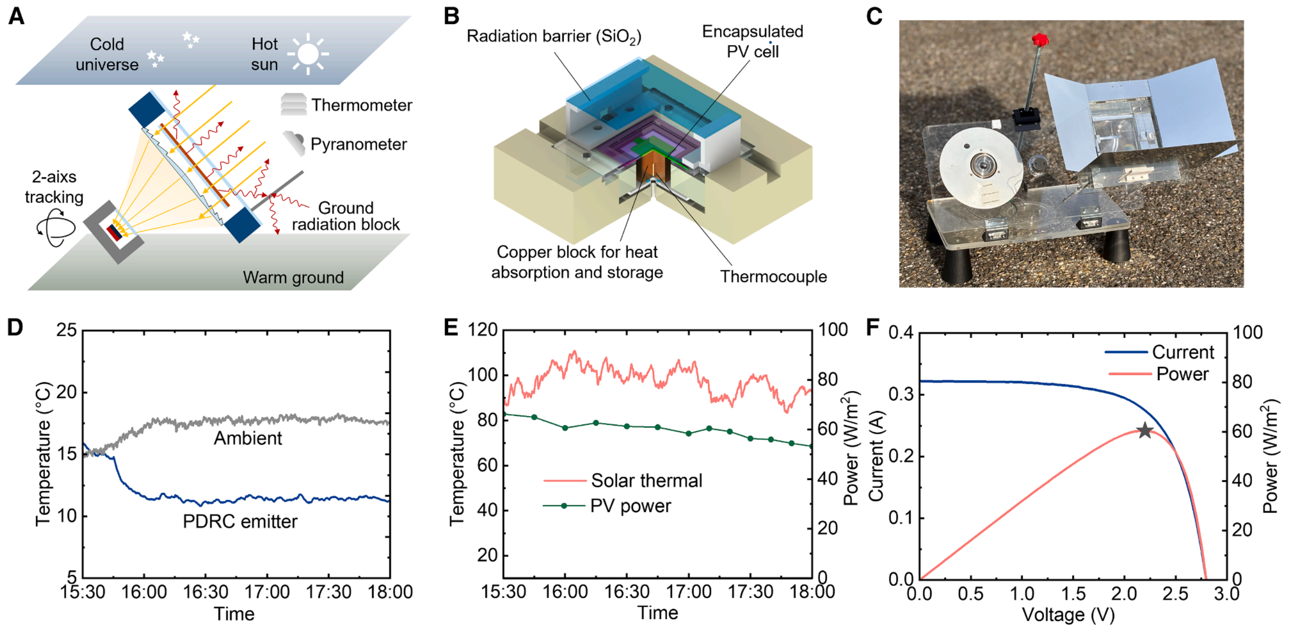


**Figure 3. Tri-generation performance of the hybrid PDRCS prototype**

(A) Schematic of the PDRCS in operation. The system tracks the sun using a two-axis platform, resulting in an inclined orientation. A mid-infrared (MIR) reflector blocks radiation from the ground.

(B) Structure of the concentrated photovoltaic-thermal collector. An encapsulated GaAs solar cell is mounted on a copper block for thermal storage, and a silica radiation barrier is positioned above the cell to reduce radiative coupling with the PDRC emitter.

(C) Photograph of the complete PDRCS prototype.

(D) Cooling performance of the PDRCS. The transparent PDRC emitter reaches a maximum of 6.5°C below ambient.

(E) Electrical and thermal performance of the concentrated photovoltaic-thermal module. The module generates 60.6 W/m$^2$ of electricity and attains a maximum temperature of 110.8°C during outdoor operation.

(F) Current-voltage and power-voltage characteristics of the GaAs cell, with the maximum power point marked by a star.

electricity, and high-temperature heat. Weather conditions during the experiment are provided in Figure S5.

The heating temperature is measured by a thermocouple embedded at the center of the copper block. The solar cell temperature can be considerably higher than the block temperature, as shown in Figure S6. The current-voltage and power-voltage characteristics of the GaAs cell are provided in Figure 3F. Although the electrical output could be further increased by using higher-performance GaAs cells and by optimizing the alignment of the cell with the Fresnel focal spot, these improvements lie beyond the scope of the present work and represent promising directions for future development of the PDRCS platform.

## Impact of solar concentration on the hybrid PDRCS performance

The solar concentration in the PDRCS confines the hot solar collector to a small area, which reduces radiative coupling with the cold PDRC emitter. Furthermore, the radiation barrier and Fresnel lens positioned between the solar collector and the PDRC emitter further block the radiative heat exchange. To quantify these effects, we compare two configurations: the concentrated design presented above (design 1) and a non-concentrated design (design 2), shown in Figures 4A and 4B. In design 2, the sunlight transmitted through the transparent PDRC emitter is not concentrated; instead, it is absorbed directly by a photovoltaic-thermal module with the same area as the PDRC emitter. The module consists of a 10 × 10-cm silicon solar cell mounted on a 10 × 10 × 1-cm copper thermal storage block.

Heat-transfer circuit models were developed for both designs (Figures 4A and 4B). Heat flows from the hot photovoltaic surface at temperature $T_h$ to the cold PDRC emitter at temperature $T_c$ and exchanges with the ambient environment at temperature $T_a$. The resistance between each surface and the ambient is governed by wind-driven convection ($R_w$). Between adjacent surfaces, the resistances ($R_0$, $R_1$, and $R_2$) include both convection and radiation. The detailed governing equations are provided in Note S1. Using this circuit analogy, we quantify the heat transfer from the solar collector and ambient to the bottom surface of the PDRC emitter, denoted $P_{tot}$, as marked in Figures 4A and 4B.

Figure 4C presents $P_{tot}$ as a function of solar collector temperature $T_h$ when $T_a = T_c = 300$ K and a wind speed of 3 m/s. In the non-concentrated design 2, $P_{tot}$ increases significantly with increasing $T_h$. Thus, raising the solar collector to high temperatures also warms the PDRC emitter, which suppresses cooling. As a result, design 2 cannot simultaneously provide sub-ambient cooling and high-temperature heat. In contrast, design 1 exhibits a much smaller $P_{tot}$, with little change even as $T_h$ increases. In design 1, the PDRC emitter and concentrated solar collector remain effectively thermally decoupled. The concentrated collector therefore has the potential to reach significantly higher

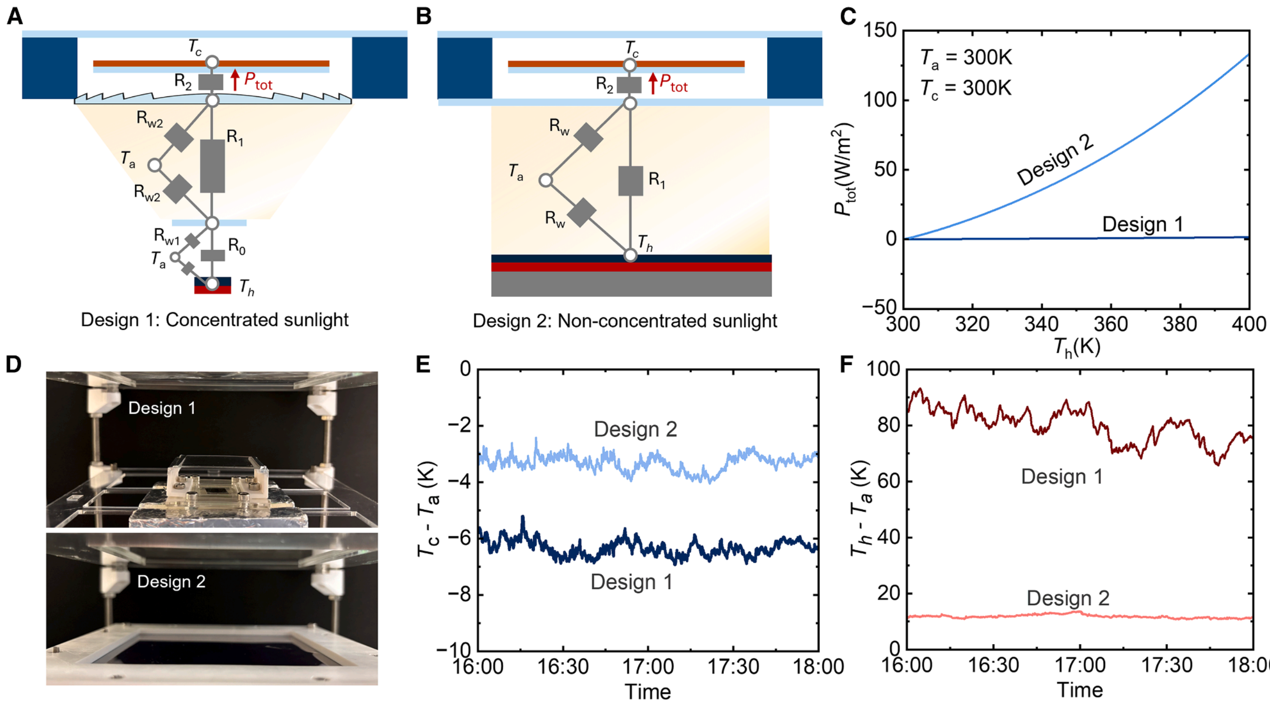


**Figure 4. Comparison between concentrated and non-concentrated PDRCS designs**

(A) Schematic of the concentrated design (design 1). Sunlight transmitted through the transparent PDRC emitter is focused onto a small-area photovoltaic-thermal collector. The corresponding heat-transfer circuit illustrates thermal pathways between the hot collector, the PDRC emitter, and the ambient.

(B) Schematic of the non-concentrated design (design 2). Sunlight passes through the transparent emitter and is absorbed by a photovoltaic-thermal collector with the same area as the PDRC emitter. The associated heat-transfer circuit is shown.

(C) Input heat flux ($P_{tot}$) from the solar collector and ambient to the PDRC emitter as a function of collector temperature $T_h$, with ambient temperature $T_a$ and emitter temperature $Tc$ both fixed at 300 K. Design 1 exhibits a much lower $P_{tot}$ than design 2, indicating stronger thermal decoupling.

(D) Photographs of design 1 and design 2. The collector area in design 1 is significantly smaller than the emitter area, whereas in design 2 both areas are equal.

(E) Cooling performance of the two designs under outdoor testing. Between 16:00 and 18:00, the PDRC emitter in design 1 maintains an average of 6.3°C below ambient, compared to 3.3°C below ambient in design 2.

(F) Heating performance of the photovoltaic-thermal collectors. Over the same interval, the concentrated collector in design 1 reaches an average of 80.0°C above ambient, while the non-concentrated collector in design 2 reaches only 11.8°C above ambient.

temperatures without degrading the cooling performance of the PDRC emitter.

To further compare the two designs, we fabricated the non-concentrated configuration (design 2). Photographs of design 1 and design 2 are shown in Figure 4D. In design 1, the photovoltaic-thermal collector occupies a much smaller area than the PDRC emitter chamber, whereas, in design 2, both components have the same area. Design 2 was tested outdoors on 9 May 2025 under weather conditions similar to those during the 7 April 2025 test of design 1, as shown in Figure S5. For a direct comparison, we evaluate the cooling and heating performance between 16:00 and 18:00, when both systems reach stable operation. In this period, the PDRC emitter in design 2 is on average 3.3°C below ambient, while the emitter in design 1 reaches an average of 6.3°C below ambient (Figure 4E). The difference is even more pronounced for heating performance: the solar collector in design 2 is only 11.8°C above ambient on average, whereas the concentrated collector in design 1 reaches 80.0°C above ambient (Figure 4F). Detailed temperature distributions of design 2 can be found in Figure S7. These simulation and experimental results confirm that the concentrated design provides far better thermal decoupling between the solar collector and the PDRC emitter. This effective decoupling allows the PDRC emitter to maintain sub-ambient cooling while the solar collector generates high-temperature heat.

Although design 1 uses a much smaller photovoltaic area than design 2, the transmitted sunlight is concentrated onto the photovoltaic cell, producing a higher solar flux density over the smaller active photovoltaic area. Under the same direct solar irradiance, the total solar energy incident on the photovoltaic cells in the two designs could therefore be comparable. In the present proof-of-concept experiments, however, design 1 produced a lower electrical output of 60.6 W/m$^2$ compared with 119.8 W/m$^2$ for design 2 (Figure S7). This difference is mainly attributed to the higher photovoltaic operating temperature in design 1, the loss of diffuse-light utilization in the concentrated optical configuration, and possible misalignment between the photovoltaic cell and the Fresnel lens focal point. Future improvements in photovoltaic-thermal management, optical alignment, and high-efficiency multi-junction concentrated solar cells

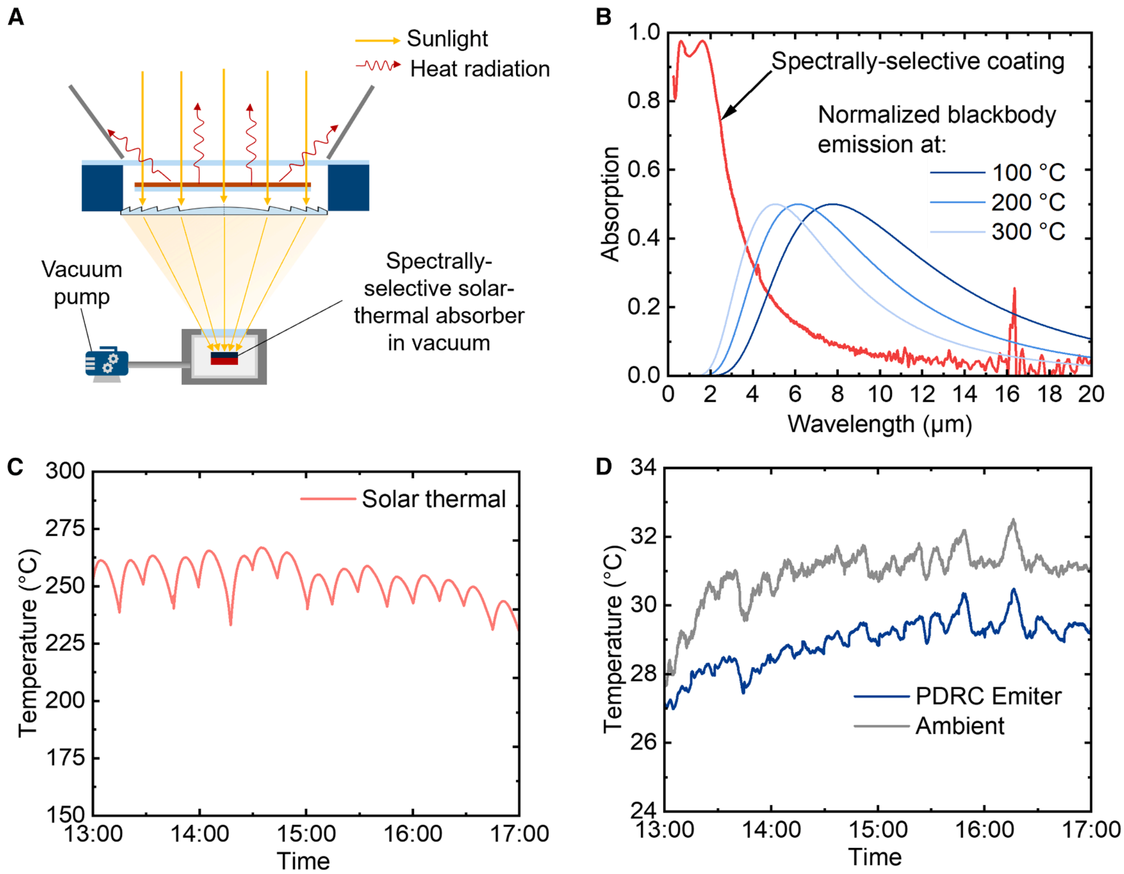


**Figure 5. Performance of the upgraded PDRCS prototype for co-generating sub-ambient cooling and higher-temperature heat**

(A) Schematic of the upgraded PDRCS prototype. A spectrally selective solar-thermal absorber replaces the photovoltaic cell to enable high-temperature heat generation. The solar collector is enclosed in a vacuum chamber to minimize convective and conductive heat losses while the transparent PDRC emitter provides sub-ambient cooling.

(B) Absorption spectrum of the spectrally selective solar-thermal absorber, together with the black-body emission curves at 100°C, 200°C, and 300°C for reference. The absorber exhibits 94% solar absorption in the 0.3- to 2.5-μm range and low emissivity of 0.08 based on the 100°C black-body spectrum and emissivity of 0.16 based on the 300°C spectrum, effectively suppressing MIR thermal emission.

(C) Heating performance of the solar-thermal absorber during outdoor testing on 19 September 2025. The absorber reaches a maximum temperature of 266.8°C at 14:35, with fluctuations caused by the solar tracker adjusting every 15 min.

(D) Cooling performance of the transparent PDRC emitter during the same period. The emitter maintains 2.4°C below ambient while the solar absorber operates at temperatures above 250°C.

could substantially increase the electrical performance of design 1 while preserving its advantages in thermal decoupling, sub-ambient cooling, and high-temperature heat generation.

## Potential for co-generating higher-temperature heat while maintaining sub-ambient cooling

To further evaluate the capability of the PDRCS to deliver higher-temperature heat from the solar collector while maintaining sub-ambient cooling from the PDRC emitter, we upgraded the prototype as shown in Figure 5A. Because photovoltaic cells are not suitable for sustained operation at elevated temperatures, the GaAs solar cell was replaced with a spectrally selective solar-thermal absorber. In addition, a vacuum pump was used to evacuate the solar collector chamber in order to minimize heat losses to the environment.

This upgraded prototype is designed solely for co-generation of cooling and high-temperature heat rather than electricity production. The aim is to assess the upper temperature limits achievable by the solar collector and to examine the degree of thermal decoupling that can be maintained between the collector and the transparent PDRC emitter under high-temperature conditions.

The absorption spectrum of the spectrally selective solar-thermal absorber from 0.3 to 20 μm is shown in Figure 5B. The absorber exhibits a high solar absorption of 94% in the 0.3- to 2.5-μm range. Its emissivity is 0.08 based on the 100°C black-body spectrum and 0.16 based on the 300°C spectrum. This strong spectral selectivity suppresses thermal radiation losses from the hot solar-thermal collector while maintaining efficient solar absorption.

The upgraded prototype was tested outdoors on 19 September 2025. The temperature of the solar-thermal absorber is presented in Figure 5C. The observed fluctuations are caused by the solar tracker, which adjusts its position every 15 min. The absorber reached a maximum temperature of 266.8°C at 14:35. The cooling performance of the transparent PDRC emitter is shown in Figure 5D. The emitter maintained a sub-ambient temperature of 2.4°C below ambient at the same time.

Our previous theoretical analysis predicts very limited thermal exchange between the PDRC emitter and the concentrated solar-thermal absorber, consistent with the observed cooling. The somewhat reduced cooling performance compared to the tri-generation experiment is mainly attributed to environmental conditions. Humidity during the 19 September 2025 test was higher, with a value of 43% at 16:00 according to Figure S5, compared to 33% at 16:00 on 7 April 2025. Higher humidity increases atmospheric thermal radiation and weakens net radiative cooling. In addition, the solar elevation angle was lower, 31° at 16:00 on 19 September compared to 37° at 16:00 on 7 April. This required the PDRCS to be tilted 6° further toward the ground, which increases the view to warm ground surfaces and reduces the effective atmospheric transmittance at low elevation angles. Overall, the results demonstrate that the thermal decoupling strategy enabled by solar concentration and spectral management allows the PDRCS to operate effectively across a wide temperature range, highlighting its potential for applications requiring both deep cooling and high-grade thermal energy from the same surface.

## DISCUSSION

This work demonstrates that a transparent PDRC emitter can operate in tandem with a concentrated solar harvesting module to deliver sub-ambient cooling, electricity generation, and high-temperature heating at the same time and from the same surface. This tri-generation strategy enables simultaneous and optimal use of universe coldness and also the full solar spectrum. In the PDRCS, solar concentration reduces the solar collector footprint and therefore the radiative view factor to the emitter, while a radiation barrier further limits thermal exchange. Together, these mechanisms establish strong thermal decoupling that allows the PDRC emitter to maintain sub-ambient cooling while the solar collector generates electricity and high-temperature heat.

Outdoor experiments validate this approach. The PDRCS achieves 6.5°C sub-ambient cooling, generates 60.6 $W/m^2$ of electricity, and reaches a collector temperature of 110.8°C under typical conditions. Comparison with a non-concentrated design highlights the importance of thermal separation; without concentration, the collector warms the emitter and limits the achievable heating temperature. The upgraded high-temperature prototype further shows that the architecture can support temperatures up to 266.8°C while maintaining 2.4°C sub-ambient cooling.

In practical applications, the heat generated by the concentrated photovoltaic-thermal module or the concentrated solar-thermal absorber can be extracted through well-developed heat-exchange technologies using suitable heat-transfer media, such as water or thermal oils.[35] The collected heat can then be stored in thermal-energy storage tanks to decouple heat generation from end-use demand. Depending on the operating temperature, this thermal output could be used for building space heating, domestic hot water, and low to medium temperature industrial processes.[36] The cooling generated by the transparent PDRC emitter can be extracted using airflow through the PDRC emitter chamber.[37] Since air is transparent to both sunlight and MIR radiation, this approach preserves solar transmission while collecting cooling from the emitter. The cooled air can be used for ventilation pre-cooling, building cooling, or as the cold stream in an air-based heat exchanger.

In the current proof-of-concept PDRCS prototype, the photovoltaic cell is thermally coupled to the copper thermal storage block to enable simultaneous electricity and heat generation. This configuration leads to elevated photovoltaic operating temperatures, which can reduce electrical efficiency and may affect long-term device stability. Therefore, for practical long-term operation, the photovoltaic cell should be maintained at a lower temperature through improved thermal management. This would improve photovoltaic stability, although the heat output temperature would be lower than that obtained in the present demonstration. An alternative route is to use a spectral-splitting photovoltaic-thermal design, in which short-wavelength photons are directed to the photovoltaic cell for electricity generation, while longer-wavelength photons are directed to a thermally decoupled solar-thermal absorber for high-temperature heat generation.[38] Such spectral-splitting photovoltaic-thermal design could be implemented using Bragg mirror optical filters,[39] semi-transparent photovoltaic cells,[40] or other wavelength-selective optical elements.[41] This approach would allow the photovoltaic cell to operate at a lower temperature while still enabling high-temperature heat generation.

To examine the potential performance of solar-transparent PDRC emitters, we simulate two idealized coolers: a solar-transparent infrared-broadband emitter that is fully transparent to sunlight and has 100% emissivity from 4 to 20 μm and a solar-transparent infrared-selective emitter that is fully transparent to sunlight and has 100% emissivity only within the atmospheric window from 8 to 13 μm. The simulation shows that the infrared-selective emitter reaches a lower stagnation temperature, approximately 16.9°C below ambient, compared with approximately 12.4°C below ambient for the infrared-broadband emitter (Figure S8). The PDMS-based transparent PDRC emitter used in this proof-of-concept study is closer to the broadband emitter because of its simple fabrication, high solar transmittance, and strong MIR emission. Future development of solar-transparent infrared-selective emitters could further improve the cooling performance of the PDRCS collector while maintaining sunlight transmission to the downstream solar collector.

Overall, these results in this study establish that co-harvesting universe coldness and solar heat is both feasible and effective. Further improvements in photovoltaic-thermal devices, emitter materials, optical alignment, and insulation could enhance electricity or heat production. Integration with thermal storage or sorption systems may extend the concept to solar-driven cooling, water harvesting, and low-temperature industrial applications. The PDRCS represents a pathway toward co-harvesting universe coldness and solar energy.

## METHODS

### Fabrication of key parts of the PDRCS prototype

#### *Transparent PDRC emitter*

A transparent radiative cooling emitter was fabricated using a polydimethylsiloxane (PDMS) elastomer (Sylgard 184, VWR). The base and curing agent were mixed in a 10:1 weight ratio in a clean beaker and stirred vigorously for 5 min to ensure homogeneity. To eliminate entrapped air bubbles, the mixture was placed in a vacuum oven (Thermo Scientific) at a pressure of ~50 mbar for 10 min. The chamber was then vented to atmospheric pressure, and the degassing cycle was repeated 2–3 times until all bubbles were visibly removed. The degassed PDMS was blade-coated onto a 1-mm-thick silica wafer (University Wafer) using an automatic film applicator. The blade gap was set to yield a PDMS film thickness of ~70 μm. The coated wafer was then placed on a digital hot plate at 100°C for 15 min to thermally cure the PDMS and achieve full crosslinking. The final emitter exhibited high optical transparency in the solar spectrum and high thermal emissivity in the MIR.

#### *Transparent PDRC emitter chamber*

A chamber was constructed from laser-cut polymethyl methacrylate (PMMA) sheets (3-mm thick) bonded with glues. The inner dimensions were 12 × 12 × 3 cm. To suppress unintended solar heating, all internal walls were lined with polished aluminum reflectors (ALANOD Miro). A 3-cm-thick closed-cell polyurethane foam was used to thermally insulate all vertical outer walls. The top surface was sealed with a stretched low-density polyethylene (LDPE) film (thickness ~50 μm, IR transparent), while the bottom was covered by a 3-mm-thick PMMA Fresnel lens to enable solar concentration.

#### *MIR reflectors*

Commercially available high-reflectivity aluminum films (ALANOD Miro) were used as MIR reflectors. These films have designed >95% reflectance in the 8- to 13-μm atmospheric window and were cut to size and affixed to the inner surfaces of the chamber using thermally stable adhesive tape.

#### *Photovoltaic-thermal collector*

The photovoltaic-thermal module consisted of a 1 × 1-cm single-junction GaAs photovoltaic cell, thermally bonded with silver paste to a 1 × 1 × 1-cm copper cube. A 0.5-mm-thick silica cover glass was placed atop the solar cell, and the entire assembly was encapsulated with optically transparent PDMS for environmental protection.

#### *Solar-thermal collector*

A 0.5-mm-thick spectrally selective solar absorber (ALANOD) was attached to a 1-cm-thick copper cube using thermal adhesive (Arctic Silver Epoxy). The absorber assembly was centrally suspended in a PMMA chamber using a silica-based frame. This frame ensured precise positioning to avoid thermal contact with chamber walls while maintaining optical alignment.

#### *Solar tracker*

A two-axis solar tracking system was constructed from laser-cut PMMA parts, 3D-printed polylactic acid (PLA) brackets, stainless steel hinges, and a 1-cm-diameter steel rod serving as the vertical rotational axis. The tracker operates manually aligned every 15 min using solar alignment marks. For experimental reproducibility, the design and 3D model files (in STL and STEP formats) are available upon request.

### Optical characterization

#### *Spectral transmittance and reflectance*

The transmittance and reflectance of the optical components (PDMS, LDPE, silica glass, etc.) were measured using a dual-beam UV-visible-near-IR spectrophotometer (Agilent Cary 7000) equipped with a 150-mm integrating sphere. Measurements were conducted in the 0.3- to 2.5-μm range. MIR spectral emissivity in the 2.5- to 25-μm range was measured using a Bruker Vertex 70 Fourier transform infrared (FTIR) spectrometer with an A562 gold-coated integrating sphere attachment. The instrument was purged with dry nitrogen to eliminate atmospheric water vapor and $CO_2$ interference. A gold mirror was used as the reference for reflectance.

### Outdoor experimental methods

Field tests were performed on the rooftop of the North Campus at Karlsruhe Institute of Technology (49.099° N, 8.437° E). The prototype was installed on the solar tracker, which was adjusted every 15 min to maintain normal incidence to the sun. Ambient air temperature was measured using a type-T thermocouple housed in a radiation shield. Total solar irradiance was recorded using an Eppley PSP pyranometer, mounted co-planar with the PDRCS surface. To differentiate direct and diffuse irradiance, a mechanical shading arm periodically blocked direct sunlight for 3 s every 15 min. Current-voltage characteristics of the GaAs photovoltaic cell were recorded using a Keithley 2618B sourcemeter. Data acquisition was automated via LabVIEW, and measurement intervals were synchronized with the solar tracker repositioning.

### Simulation methods

Thermal modeling of the PDRCS system was conducted using the heat-transfer-circuit analogy method, incorporating conductive, convective, and radiative resistances between system layers. The model includes material properties, view factor-based radiation exchange, and equivalent thermal resistances. Detailed governing equations, boundary conditions, and validation procedures are described in Note S1.

## RESOURCE AVAILABILITY

### Lead contact

Requests for further information and resources should be directed to and will be fulfilled by the lead contact, Dr. Gan Huang (gan.huang@kit.edu).

### Materials availability

This study did not generate any new unique reagents.

### Data and code availability

- All data reported in this paper will be shared by the lead contact upon request.
- This paper does not report original code for the key results.
- Any additional information required to reanalyze the data reported in this paper is available from the lead contact upon request.

## ACKNOWLEDGMENTS

The authors gratefully acknowledge financial support received from (1) the Initiative and Networking Fund of the Helmholtz Association under the call Helmholtz Investigator Group (VH-NG-21-07, UNICOS) to G.H.; (2) the Helmholtz Association Research Field Energy, Program Materials and Technologies for the Energy Transition (Topic 1 photovoltaics and wind energy, ref. 38.01.04) to G.H.; (3) the Karlsruhe School of Optics and Photonics (KSOP) to G.H. and I.A.C.G.; and (4) the US Department of Energy (grant no. DE-FG02-07ER46426) to S.F. The authors thank Mr. Sezen Su and Ms. Haiying Cheng for their support on optical characterization. The authors also thank Prof. Bryce S. Richards at Karlsruhe Institute of Technology for valuable discussion.

## AUTHOR CONTRIBUTIONS

Conceptualization, G.H. and S.F.; funding acquisition, G.H.; investigation, I.A.C.G., B.L., S.F., and G.H.; methodology, G.H., I.A.C.G., and S.F.; project administration, G.H.; supervision, G.H. and S.F.; visualization, I.A.C.G. and G.H.; writing – original draft, I.A.C.G., G.H., and S.F.; writing – review and editing, G.H., I.A.C.G., B.L., and S.F.

## DECLARATION OF INTERESTS

The authors declare no competing interests.

## SUPPLEMENTAL INFORMATION

Supplemental data related to this article can be found online at https://doi.org/10.1016/j.xcrp.2026.103492.

Received: March 6, 2026
Revised: June 10, 2026
Accepted: July 22, 2026
Published: August 13, 2026

## REFERENCES

1. (2025). The Energy Sector Is Central to Efforts to Combat Climate Change (International Energy Agency). https://www.iea.org/spotlights/the-energy-sector-is-central-to-efforts-to-combat-climate-change.
2. (2025). Buildings (International Energy Agency). https://www.iea.org/energy-system/buildings#programmes.
3. Berardi, U. (2015). Building energy consumption in US, EU, and BRIC countries. Procedia Eng. *118*, 128–136. https://doi.org/10.1016/j.proeng.2015.08.411.
4. Photovoltaics Report, Fraunhofer ISE, 2025.
5. Wang, Z., Kortge, D., Zhu, J., Zhou, Z., Torsina, H., Lee, C., and Bermel, P. (2020). Lightweight, passive radiative cooling to enhance concentrating photovoltaics. Joule *4*, 2702–2717. https://doi.org/10.1016/j.joule.2020.10.004.
6. (2025). Renewables 2025 (International Energy Agency). https://www.iea.org/reports/renewables-2025.
7. Herrando, M., Wang, K., Huang, G., Otanicar, T., Mousa, O.B., Agathokleous, R.A., Ding, Y., Kalogirou, S., Ekins-Daukes, N., Taylor, R.A., et al. (2023). A review of solar hybrid photovoltaic-thermal (PV-T) collectors and systems. Prog. Energy Combust. Sci. *97*, 101072. https://doi.org/10.1016/j.pecs.2023.101072.
8. Fan, S., and Li, W. (2022). Photonics and thermodynamics concepts in radiative cooling. Nat. Photonics *16*, 182–190. https://doi.org/10.1038/s41566-021-00921-9.
9. Yin, X., Yang, R., Tan, G., and Fan, S. (2020). Terrestrial radiative cooling: Using the cold universe as a renewable and sustainable energy source. Science *370*, 786–791. https://doi.org/10.1126/science.abb0971.
10. Raman, A.P., Anoma, M.A., Zhu, L., Rephaeli, E., and Fan, S. (2014). Passive radiative cooling below ambient air temperature under direct sunlight. Nature *515*, 540–544. https://doi.org/10.1038/nature13883.
11. Shi, N.N., Tsai, C.C., Camino, F., Bernard, G.D., Yu, N., and Wehner, R. (2015). Keeping cool: Enhanced optical reflection and radiative heat dissipation in Saharan silver ants. Science *349*, 298–301. https://doi.org/10.1126/science.aab3564.
12. Zhao, B., Hu, M., Ao, X., Chen, N., and Pei, G. (2019). Radiative cooling: A review of fundamentals, materials, applications, and prospects. Appl. Energy *236*, 489–513. https://doi.org/10.1016/j.apenergy.2018.12.018.
13. Liu, R., Wang, S., Zhou, Z., Zhang, K., Wang, G., Chen, C., and Long, Y. (2025). Materials in radiative cooling technologies. Adv. Mater. *37*, 2401577. https://doi.org/10.1002/adma.202401577.
14. Wang, C., Chen, H., and Wang, F. (2024). Passive daytime radiative cooling materials toward real-world applications. Prog. Mater. Sci. *144*, 101276. https://doi.org/10.1016/j.pmatsci.2024.101276.
15. Lin, C., Li, K., Li, M., Dopphoopha, B., Zheng, J., Wang, J., Du, S., Li, Y., Huang, B., and Huang, B. (2025). Pushing radiative cooling technology to real applications. Adv. Mater. *37*, 2409738. https://doi.org/10.1002/adma.202409738.
16. Zhai, Y., Ma, Y., David, S.N., Zhao, D., Lou, R., Tan, G., Yang, R., Yin, X., and Yin, X. (2017). Scalable-manufactured randomized glass-polymer hybrid metamaterial for daytime radiative cooling. Science *355*, 1062–1066. https://doi.org/10.1126/science.aai7899.
17. Zhou, L., Song, H., Liang, J., Singer, M., Zhou, M., Stegenburgs, E., Zhang, N., Xu, C., Ng, T., Yu, Z., et al. (2019). A polydimethylsiloxane-coated metal structure for all-day radiative cooling. Nat. Sustain. *2*, 718–724. https://doi.org/10.1038/s41893-019-0348-5.
18. Mandal, J., Fu, Y., Overvig, A.C., Jia, M., Sun, K., Shi, N.N., Zhou, H., Xiao, X., Yu, N., Yang, Y., and Yang, Y. (2018). Hierarchically porous polymer coatings for highly efficient passive daytime radiative cooling. Science *362*, 315–319. https://doi.org/10.1126/science.aat9513.
19. Guo, C., Tang, H., Wang, P., Xu, Q., Pan, H., Zhao, X., Fan, F., Li, T., Zhao, D., and Zhao, D. (2024). Radiative cooling assisted self-sustaining and highly efficient moisture energy harvesting. Nat. Commun. *15*, 6100. https://doi.org/10.1038/s41467-024-50396-9.
20. Mandal, J., Jia, M., Overvig, A., Fu, Y., Che, E., Yu, N., and Yang, Y. (2019). Porous polymers with switchable optical transmittance for optical and thermal regulation. Joule *3*, 3088–3099. https://doi.org/10.1016/j.joule.2019.09.016.
21. Wu, R., Sui, C., Chen, T.H., Zhou, Z., Li, Q., Yan, G., Han, Y., Liang, J., Hung, P.J., Luo, E., et al. (2024). Spectrally engineered textile for radiative cooling against urban heat islands. Science *384*, 1203–1212. https://doi.org/10.1126/science.adl0653.
22. Wu, X., Li, J., Jiang, Q., Zhang, W., Wang, B., Li, R., Zhao, S., Wang, F., Huang, Y., Lyu, P., et al. (2023). An all-weather radiative human body cooling textile. Nat. Sustain. *6*, 1446–1454. https://doi.org/10.1038/s41893-023-01200-x.
23. Cai, L., Peng, Y., Xu, J., Zhou, C., Zhou, C., Wu, P., Lin, D., Fan, S., Cui, Y., and Cui, Y. (2019). Temperature regulation in colored infrared-transparent polyethylene textiles. Joule *3*, 1478–1486. https://doi.org/10.1016/j.joule.2019.03.015.
24. Lin, K., Chen, S., Zeng, Y., Ho, T.C., Zhu, Y., Wang, X., Liu, F., Huang, B., Chao, C.Y.H., Wang, Z., et al. (2023). Hierarchically structured passive radiative cooling ceramic with high solar reflectivity. Science *382*, 691–697. https://doi.org/10.1126/science.adi4725.
25. Zhao, X., Li, T., Xie, H., Liu, H., Wang, L., Qu, Y., Li, S.C., Liu, S., Brozena, A.H., Yu, Z., et al. (2023). A solution-processed radiative cooling glass. Science *382*, 684–691. https://doi.org/10.1126/science.adi2224.
26. Xie, F., Jin, W., Nolen, J.R., Pan, H., Yi, N., An, Y., Zhang, Z., Kong, X., Zhu, F., Jiang, K., et al. (2024). Subambient daytime radiative cooling of vertical surfaces. Science *386*, 788–794. https://doi.org/10.1126/science.adn2524.

27. Zhou, J., Chen, T.G., Tsurimaki, Y., Hajj-Ahmad, A., Fan, L., Peng, Y., Xu, R., Wu, Y., Assawaworrarit, S., Fan, S., et al. (2023). Angle-selective thermal emitter for directional radiative cooling and heating. Joule *7*, 2830–2844. https://doi.org/10.1016/j.joule.2023.10.013.

28. Li, X., Sun, B., Sui, C., Nandi, A., Fang, H., Peng, Y., Tan, G., Hsu, P.C., and Hsu, P.C. (2020). Integration of daytime radiative cooling and solar heating for year-round energy saving in buildings. Nat. Commun. *11*, 6101. https://doi.org/10.1038/s41467-020-19790-x.

29. Li, W., Buddhiraju, S., and Fan, S. (2020). Thermodynamic limits for simultaneous energy harvesting from the hot sun and cold outer space. Light Sci. Appl. *9*, 68. https://doi.org/10.1038/s41377-020-0296-x.

30. Chen, Z., Zhu, L., Li, W., and Fan, S. (2019). Simultaneously and synergistically harvest energy from the sun and outer space. Joule *3*, 101–110. https://doi.org/10.1016/j.joule.2018.10.009.

31. Zhou, L., Song, H., Zhang, N., Rada, J., Singer, M., Zhang, H., Ooi, B.S., Yu, Z., Gan, Q., and Gan, Q. (2021). Hybrid concentrated radiative cooling and solar heating in a single system. Cell Rep. Phys. Sci. *2*, 100338. https://doi.org/10.1016/j.xcrp.2021.100338.

32. Hu, M., Zhao, B., Cao, J., Cao, J., Wang, Q., Riffat, S., Su, Y., and Pei, G. (2021). Feasibility of realizing daytime solar heating and radiative cooling simultaneously with a novel structure. Sustain. Cities Soc. *74*, 103224. https://doi.org/10.1016/j.scs.2021.103224.

33. Ghosh, P., Wei, X., Liu, H., Zhang, Z., and Zhu, L. (2024). Simultaneous subambient daytime radiative cooling and photovoltaic power generation from the same area. Cell Rep. Phys. Sci. *5*, 101876. https://doi.org/10.1016/j.xcrp.2024.101876.

34. Huang, G., Yengannagari, A.R., Matsumori, K., Patel, P., Datla, A., Trindade, K., Amarsanaa, E., Zhao, T., Köhler, U., Busko, D., et al. (2024). Radiative cooling and indoor light management enabled by a transparent and self-cleaning polymer-based metamaterial. Nat. Commun. *15*, 3798. https://doi.org/10.1038/s41467-024-48150-2.

35. Chow, T.T. (2018). A review on photovoltaic/thermal hybrid solar technology. Renew. Energy *4*, 88–119.

36. Tian, Y., and Zhao, C.Y. (2013). A review of solar collectors and thermal energy storage in solar thermal applications. Appl. Energy *104*, 538–553. https://doi.org/10.1016/j.apenergy.2012.11.051.

37. Jia, S., Huang, M., Jiang, X., Shen, C., Chen, S., Meng, G., Li, X., Guo, W., and Guo, W. (2025). Tandem daytime radiative cooling and solar power generation. Cell Rep. Phys. Sci. *6*, 102343. https://doi.org/10.1016/j.xcrp.2024.102343.

38. Crisostomo, F., Taylor, R.A., Surjadi, D., Mojiri, A., Rosengarten, G., and Hawkes, E.R. (2015). Spectral splitting strategy and optical model for the development of a concentrating hybrid PV/T collector. Appl. Energy *141*, 238–246. https://doi.org/10.1016/j.apenergy.2014.12.044.

39. Lehmann, B., and Huang, G. (2026). Hybrid solar collectors based on Bragg-mirror spectral splitting for simultaneous heat and electricity generation. Sol. Energy *306*, 114288. https://doi.org/10.1016/j.solener.2025.114288.

40. Huang, G., Arya, P.H., Ritzer, D.B., Alati, N.A., Abdollahi Nejand, B., Paetzold, U.W., and Richards, B.S. (2025). Hybrid Perovskite-Photovoltaic and Solar-Thermal Harvesting. Adv. Sci. *12*, e09692. https://doi.org/10.1002/advs.202509692.

41. Lehmann, B., Richards, B.S., and Huang, G. (2026). Spectral-Splitting Photovoltaic-Thermal Solar Collectors Using Selective Hybrid Liquid-Solid Optical Filters. Adv. Opt. Mater. *14*, e02756. https://doi.org/10.1002/adom.202502756.